PHYSICAL REVIEW C **92**, 054607 (2015)

Scaling violation and relativistic effective mass from quasi-elastic electron scattering: Implications for neutrino reactions

J. E. Amaro,[*] E. Ruiz Arriola,[†] and I. Ruiz Simo[‡]

Departamento de Física Atómica, Molecular y Nuclear and Instituto Carlos I de Física Teórica y Computacional Universidad de Granada, E-18071 Granada, Spain

(Received 20 May 2015; revised manuscript received 29 June 2015; published 10 November 2015)

The experimental data from quasi-elastic electron scattering from ^{12}C are reanalyzed in terms of a new scaling variable suggested by the interacting relativistic Fermi gas with scalar and vector interactions, which is known to generate a relativistic effective mass for the interacting nucleons. By choosing a mean value of this relativistic effective mass $m_N^* = 0.8m_N$, we observe that most of the data fall inside a region around the inverse parabola-shaped universal scaling function of the relativistic Fermi gas. This suggests a method to select the subset of data that highlight the quasi-elastic region, about two thirds of the total 2500 data. Regardless of the momentum and energy transfer, this method automatically excludes the data that are not dominated by the quasi-elastic process. The resulting band of data reflects deviations from perfect universality and can be used to characterize experimentally the quasi-elastic peak, despite the manifest scaling violation. Moreover, we show that the spread of the data around the scaling function can be interpreted as genuine fluctuations of the effective mass $M^* \equiv m_N^*/m_N \sim 0.8 \pm 0.1$. Applying the same procedure we transport the scaling quasi-elastic band into a theoretical prediction band for the neutrino-scattering cross section that is compatible with the recent measurements and slightly more accurate.

DOI: 10.1103/PhysRevC.92.054607 PACS number(s): 24.10.Jv, 25.30.Fj, 25.30.Pt, 21.30.Fe

I. INTRODUCTION

Quasielastic (QE) electron scattering from nuclei has experienced a revival from the practical need to gauge the validity of the current models as applied to neutrino scattering and oscillation experiments [1–5] (for recent reviews see Refs. [6–9]). The conventional approach pursues a detailed microscopic relativistic description of the inelastic processes and then requires all the relevant mechanisms for the particular Q^2 kinematics. At present there is no compelling model able to describe the world (e,e') experiments. In the case of ^{12}C, taken as example here, the more than 2500 data available spread over a huge (q,ω) kinematical region, reaching well inside the relativistic regime. A crucial issue is to find which electron data encode the maximum information to be applied to neutrino scattering minimizing the systematic and theoretical uncertainties in the relevant channel (quasi-elastic, pion emission, ...). The scaling approach provides an appealing and unified framework to encompass coherently the large diversity of data stemming from different experiments and kinematics. In particular the superscaling approach (SuSA) has been implemented along these lines to predict neutrino-scattering cross sections from a longitudinal scaling function $f_L(\psi')$ fit to electron data [10]. Moreover, the recent upgrade of the SuSA-v2 [11] includes nuclear effects which are theoretically inspired in a particular realization of the relativistic mean-field (RMF) theory, by an additional transverse scaling function $f_T(\psi')$ which is different from $f_L(\psi')$.

A peculiar feature of the RMF is that it is the only approach which reproduces the experimental scaling function $f_L(\psi')$ for all the values of q after an *ad hoc* q-dependent shift in energy is applied [12]. The theoretical origin of this phenomenological shift has not been well understood [11]. This model incorporates a dynamical enhancement of lower Dirac components, which is transmitted to the transverse response, R_T, improving the agreement with experimental data. However, gauge invariance is violated and hence R_T still presents ambiguities [13]. Another difficulty of the RMF and other finite nuclei models is that they break translational invariance (attempts to restore it in a relativistic system were explored in Refs. [14,15]).

The goal of this paper is to exploit the scaling idea from a novel point of view connecting the RMF with the universal scaling function of the relativistic Fermi gas (RFG)

$$f(\psi^*) = \tfrac{3}{4}(1-\psi^{*2})\theta(1-\psi^{*2}). \tag{1}$$

Rather than constructing a yet-undetermined scaling function we aim to propose a new scaling variable ψ^* mapping the data into a region around the above function. Inspired by the fact that the mean-field theory provides a consistent and reasonable description of the nuclear response in the quasi-elastic region (already observed by Rosenfelder 35 years ago [16]) for a range of kinematics, we propose to start from the interacting RFG [17] including suitable vector and scalar potentials which are inferred from the data into an effective mass m_N^* that gets reduced in the nuclear medium. The effective mass encodes relativistic dynamical effects relevant in this kinematical region, alternative to other approaches like the one based on the spectral function [18,19]. In fact, one of the motivations of our approach, called here M^* scaling (or M*S), was to provide a framework enjoying the good features of the RMF without incurring into the above-mentioned difficulties, unveiling the

[*]amaro@ugr.es
[†]earriola@ugr.es
[‡]ruizsig@ugr.es

m_N^* origin of the dynamical enhancement of both the lower components and the transverse response function. The shift of $f_L(\psi')$ is trivially obtained as a consequence of the m^* dependence of the quasi-elastic peak position.

Of course, there have been numerous attempts to determine the effective mass [20,21], but this depends on details of the dynamics. Thus, by proceeding directly from the data we avoid specifying the mean field explicitly. On the other hand, a phenomenological determination of m_N^* suffers from the uncertainties on the bulk of the data which should contribute most significantly. Therefore, we will from the beginning accept that this effective mass is determined up to a sensible uncertainty, defined precisely by a suitable selection of the large database, to be explained below in detail. One of the main advantages of this rather simple approach is not only its ease of implementation, but also that we are free from the traditional objections regarding gauge invariance or violations of partially conserved axial vector current (PCAC). We expect in this way to account for the most relevant uncertainties regarding the predictive power of the model.

II. FORMALISM

We follow closely the notation introduced in Ref. [22]. The quasi-elastic electroweak cross section is proportional to the hadronic tensor or response function for single-nucleon excitations transferring momentum $\mathbf{q}$ and energy ω, which in the Fermi gas reads

$$W^{\mu\nu}(q,\omega) = \frac{V}{(2\pi)^3}\int d^3p\,\delta(E'-E-\omega)\frac{(m_N^*)^2}{EE'} \times 2w^{\mu\nu}_{\text{s.n.}}(\mathbf{p}',\mathbf{p})\theta(k_F-p)\theta(p'-k_F), \quad (2)$$

where $E=(\mathbf{p}^2+m_N^{*\,2})^{1/2}$ is the initial nucleon energy in the mean field. The final momentum of the nucleon is $\mathbf{p}'=\mathbf{p}+\mathbf{q}$ and its energy is $E'=(\mathbf{p}'^2+m_N^{*\,2})^{1/2}$. Note that initial and final nucleons have the same effective mass m_N^*. The volume $V=3\pi^2N/k_F^3$ of the system is related to the Fermi momentum k_F and proportional to the number N of protons and/or neutrons participating in the process. Finally, the electroweak interaction mechanism is implicit in the single-nucleon tensor:

$$w^{\mu\nu}_{\text{s.n.}}(\mathbf{p}',\mathbf{p}) = \frac{1}{2}\sum_{ss'} J^{\mu *}(\mathbf{p}',\mathbf{p})J^{\nu}(\mathbf{p}',\mathbf{p}), \quad (3)$$

where $J^{\mu *}$ is the electroweak current matrix element between free positive-energy Dirac spinors, with mass m_N^* and normalized to $\overline{u}u=1$. In the case of electron scattering we are involved with the electromagnetic current matrix element

$$J^{\mu}_{s's}(\mathbf{p}',\mathbf{p}) = \overline{u}_{s'}(\mathbf{p}')\left[F_1(Q^2)\gamma^\mu + F_2(Q^2)i\sigma^{\mu\nu}\frac{Q_\nu}{2m_N}\right]u_s(\mathbf{p}), \quad (4)$$

where F_1 and F_2 are, respectively, the Dirac and Pauli electromagnetic form factors of proton or neutron.

In the case of (e,e') the quasi-elastic cross section is written in Rosenbluth form

$$\frac{d\sigma}{d\Omega' d\epsilon'} = \sigma_{\text{Mott}}(v_L R_L + v_T R_T), \quad (5)$$

where σ_{Mott} is the Mott cross section, $v_L = Q^4/q^4$, and $v_T = \tan^2(\theta/2) - Q^2/(2q^2)$, with θ being the scattering angle. The nuclear longitudinal and transverse response functions are the following components of the hadronic tensor in a coordinate system with the z axis in the $\mathbf{q}$ direction (longitudinal):

$$R_L(q,\omega) = W^{00}, \quad (6)$$

$$R_T(q,\omega) = W^{11} + W^{22}. \quad (7)$$

In the RFG the nuclear response functions can be written in the factorized form for $K = L,T$ as

$$R_K = G_K f(\psi^*), \quad (8)$$

$$G_K = \Lambda\left(ZU_K^p + NU_K^n\right), \quad (9)$$

where $f(\psi^*)$ is given in Eq. (1) and ψ^* is defined below. Moreover,

$$\Lambda = \frac{\xi_F}{m_N^*\eta_F^3\kappa}, \quad (10)$$

and the single-nucleon response functions are

$$U_L = \frac{\kappa^2}{\tau}\left[(G_E^*)^2 + \frac{(G_E^*)^2+\tau(G_M^*)^2}{1+\tau}\Delta\right], \quad (11)$$

$$U_T = 2\tau(G_M^*)^2 + \frac{(G_E^*)^2+\tau(G_M^*)^2}{1+\tau}\Delta, \quad (12)$$

where the quantity Δ has been introduced:

$$\Delta = \frac{\tau}{\kappa^2}\xi_F(1-\psi^{*2})\left[\kappa\sqrt{1+\frac{1}{\tau}} + \frac{\xi_F}{3}(1-\psi^{*2})\right]. \quad (13)$$

Dimensionless variables have been introduced measuring the energy and momentum in units of m_N^*; namely, $\lambda = \omega/(2m_N^*)$, $\kappa = q/(2m_N^*)$, $\tau = \kappa^2 - \lambda^2$, $\eta_F = k_F/m_N^*$, and $\xi_F = (1+\eta_F^2)^{1/2} - 1$. Note that usually [22] these variables are defined with respect to the nucleon mass m_N instead of the m_N^*. The same can be said with respect to the electric and magnetic form factors, which are modified in the medium due to the effective mass according to

$$G_E^* = F_1 - \tau\frac{m_N^*}{m_N}F_2, \quad (14)$$

$$G_M^* = F_1 + \frac{m_N^*}{m_N}F_2. \quad (15)$$

One should still stress that F_1 and F_2 can depend on M^* [23]. We stick here to the phenomenologically successful CC2 prescription that reproduces the experimental superscaling function [13]. Using the CC1 operator obtained through the Gordon reduction produces the same effects as in the RMF of Ref. [13]. The same modification of form factors in the medium was explored in Ref. [24]. For the free form factors we use the Galster parametrization.

To define the scaling variable ψ^*, we first introduce the minimum energy allowed for a nucleon inside the nucleus to absorb the virtual photon (in units of m_N^*):

$$\epsilon_0 = \text{Max}\left\{\kappa\sqrt{1+\frac{1}{\tau}} - \lambda, \epsilon_F - 2\lambda\right\}, \tag{16}$$

where $\epsilon_F = (1+\eta_F^2)^{1/2}$ is the Fermi energy in units of m_N^*. The scaling variable is defined by

$$\psi^* = \sqrt{\frac{\epsilon_0 - 1}{\epsilon_F - 1}}\text{sgn}(\lambda - \tau). \tag{17}$$

Note that $\psi^* < 0$ for $\lambda < \tau$ (the left side of the quasi-elastic peak). The meaning of ψ^{*2} is the following: it is the minimum kinetic energy of the initial nucleon divided by the kinetic Fermi energy.

III. RESULTS

Starting with the experimental (e,e') cross section we compute the experimental scaling function f_{expt}

$$f_{\text{expt}} = \frac{\left(\frac{d\sigma}{d\Omega' d\epsilon'}\right)_{\text{expt}}}{\sigma_{\text{Mott}}(v_L G_L + v_T G_T)}, \tag{18}$$

which would correspond to the function $f(\psi^*)$ in the relativistic Fermi gas model.

We summarize the results of our M*S analysis in Fig. 1(a). We plot the experimental scaling function for the bulk of ^{12}C data [25,26] as a function of the scaling variable ψ^*. We take

$$M^* = \frac{m_N^*}{m_N} = 0.8. \tag{19}$$

We see that a large fraction of the data collapse into a data cloud surrounding the RFG scaling function, given by Eq. (1). Other choices of m_N^* are possible but the clustering substantially detunes from the RFG. So we interpret this pattern as the kinematic regions highlighting the effective Fermi-gas behavior of the data. This collapse of data resolves two issues simultaneously: On the theoretical side it provides an operational definition of the relativistic effective mass, whereas on the experimental side provides an operational definition of the quasi-elastic peak behavior.

The observed scaling is not perfect in the sense that the blur of data presents a finite width, but the width is roughly homogeneous as seen in Fig. 2. There we select the data that are clustered on a coarse-grain scale according to a method inspired by the visual and conventional Gaussian low-pass filtering (Gaussian blur) [27]. Due to the discrete, heterogeneous, and finite nature of the data in our case we use instead a constant weighting function. This function measures the density of points clustered above a given threshold m, inside a circle of radius r centered at the experimental point, plus minus the experimental error. In the figure we show four situations corresponding to $r = 0.1$, and for illustration the result of applying our low-pass filtering method to four values of $m = 20,\ 25,\ 30$, and 40. The parameter m measures the minimum number of experimental points surrounding each datum in the cloud. Note that we discard the surrounding points that do not verify the above condition. As we can see the shape defined by the data cloud, seen as a shaded band in the scale of the figure, presents a stable pattern around the relativistic Fermi gas when the threshold value increases, even if the number of surviving points decreases. This stability around the Fermi-gas result is triggered by the chosen value of M^*. Note that the number of data involved in these plots is around 1500, but the scaling violation (defined as the width of the shaded band) is manifest.

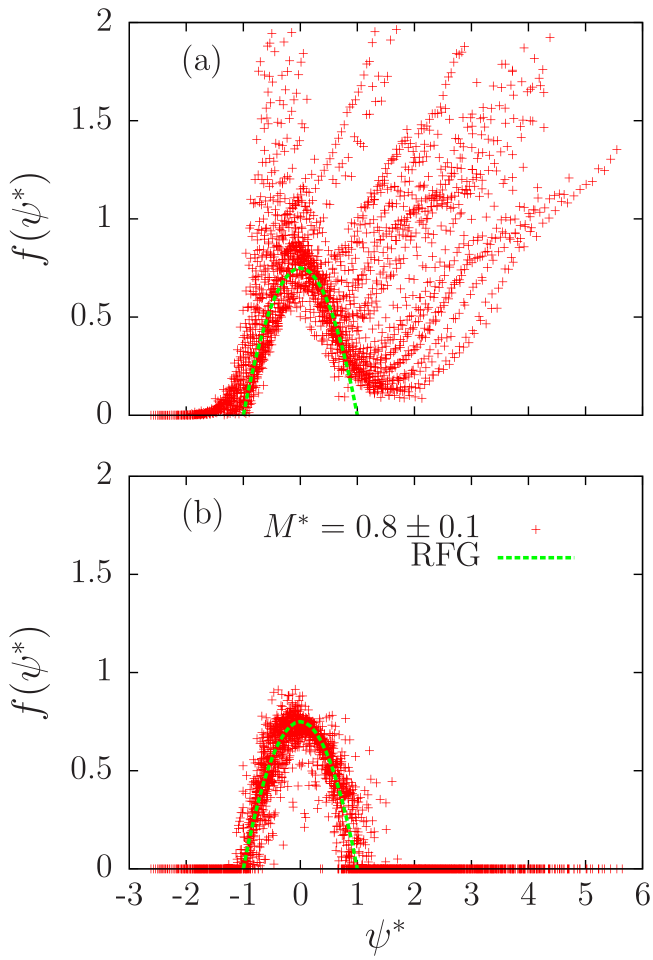

FIG. 1. (Color online) (a) M^* scaling analysis of the experimental data of ^{12}C as a function of the scaling variable ψ^* for $M^* = m_N^*/m_N = 0.8$ compared to the RFG parabola. (b) RFG Monte Carlo simulation of QE data with a Gaussian distribution of relativistic effective mass quotient around $M^* = 0.8 \pm 0.1$. The Fermi momentum is fixed to $k_F = 225$ MeV/c.

This pattern in the M*S plot, which emerges as a realization of a universal quasi-elastic peak, is a global property of the set of data and suggests an alternative interpretation in terms of fluctuations of M^*. One could propose a statistical model where each point in the cloud samples a quasi-elastic event with a slightly different effective mass around the mean value 0.8. This fluctuation does not simulate the nuclear effects beyond the impulse approximation (finite-size effects, short-range NN correlations, long-range RPA, meson-exchange currents, Δ excitation, pion emission, two-particle emission, final-state interaction). However the fluctuations are of the same order of magnitude as these effects. Actually they are

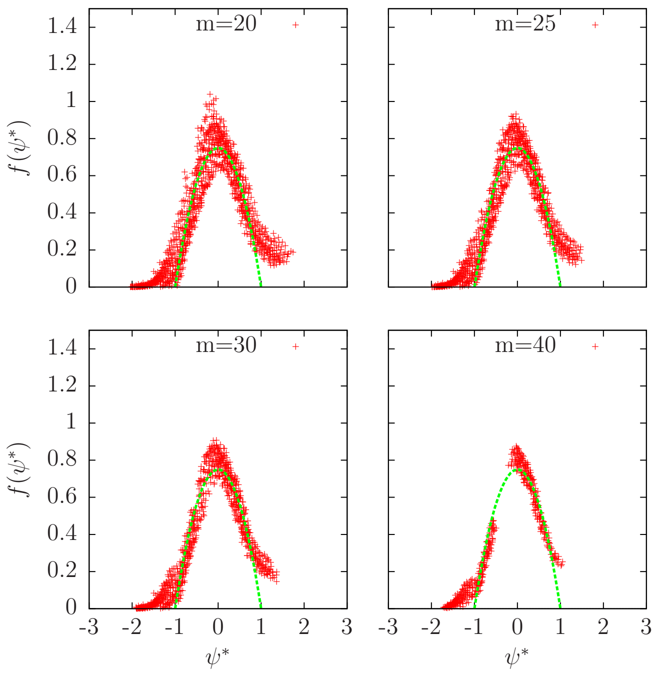

FIG. 2. (Color online) Experimental data selection in terms of the scaling variable ψ^*, obtained with different choices of the number m of points inside a circle with radius $r = 0.1$.

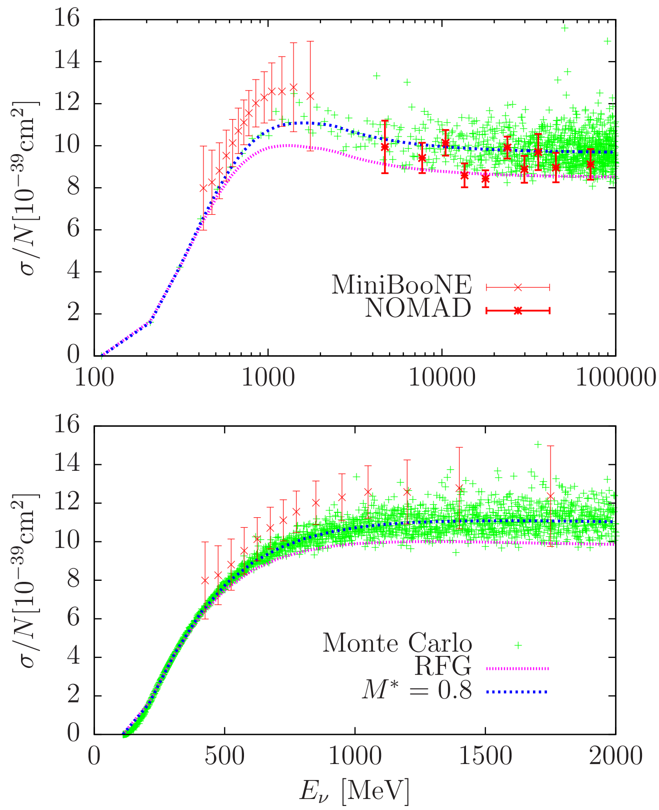

FIG. 3. (Color online) Total QE neutrino cross section of ^{12}C per neutron as a function of the neutrino energy for different relativistic effective masses generated in a Monte Carlo simulation. The experimental data are from NOMAD [1] and MiniBooNE [2]. We take the axial dipole mass $M_A = 1$ GeV.

small enough to retain the points in the neighborhood of the quasi-elastic region, which could be treated perturbatively in a microscopic framework beyond the RFG. The largest deviations of the quasi-elastic cloud from the perfect parabola occur only around its edges, where the Fermi gas is zero and hence the resulting signal cannot be accounted for by a change of m_N^*.

To justify the above assumption, we carried out a calculation by using a family of RFGs with slightly different m_N^* to generate a random point for each single experimental datum at the very same kinematics. Thus we take a random M^* around the optimal mean value 0.8 in a Monte Carlo sampling. The results of this simulation are shown in Fig. 1(b). To generate the pseudodata we use a Gaussian distribution with a width $\sigma = 0.1$, representing the fluctuation of $M^* = 0.8 \pm 0.1$, which nicely resembles the fluctuations seen in the cloud of the experimental data. This procedure automatically selects those pseudodata attributable to genuine quasi-elastic interpretation (based on the Fermi-gas definition) and zeros those kinematics that are forbidden.

Our main observation is that, by choosing the optimum relativistic effective mass, a RFG-like scaling of the data can be obtained in the quasi-elastic region, covering more than 1500 data. This implies a tradeoff between the experimental uncertainty to what extent a datum is close to quasi-elastic and the importance of the physical effects beyond the impulse approximation that contribute to the quasi-elastic mechanism. With this procedure a way to estimate what information is contained in the data about the quasi-elastic peak emerges.

From our analysis a phenomenological scaling function could be also obtained exactly in the same way as in the superscaling analysis. We have not tried to parametrize this function, which could be done from the data of Fig. 2. The resulting scaling function is asymmetrical and very similar to the longitudinal superscaling function, but with a different normalization, including the tail. Therefore the tail of the scaling function is a property of the quasi-elastic interaction.

The information extracted here about the quasi-elastic (e,e') cross section of ^{12}C can be straightforwardly used to readily make predictions for other reactions like CC neutrino scattering from the same nucleus. In Fig. 3 we show the calculations of the (ν_μ,μ^-) cross section as a function of incident neutrino energy. There we show the effective RFG results with $m_N^* = 0.8 m_N$. The cloud of points correspond to incorporating the same fluctuations ± 0.1 of M^* as in the Monte Carlo simulation depicted in Fig. 1(b). For comparison we also show the results of the conventional RFG. The effective mass produces an enhancement of the lower Dirac components, and hence also of both the vector and axial transverse responses, and of the theoretical cross section, which, thanks to the fluctuations, becomes compatible with the data for all the kinematics. In our case the fluctuations of the theoretical band are about 10%, as naively expected from the input uncertainty of the effective mass. We note that the sampling in the lower panel of Fig. 3 uses a smaller binning of 1 MeV as opposed to the upper panel where 100 MeV is used instead. The clustering of these equidistant binnings arises naturally from the log scale.

For high Q the vector form factors deviate from the conventional dipole behavior [28], which could affect, in principle, any model's predictions. However, this would only be appreciable in the differential cross section; the integrated σ, even for NOMAD kinematics, is only sensitive to the kinematical regions where the product of form factors and phase space is large. We have numerically checked that the contribution from Q^2 above 1 to 2 $(\mathrm{GeV}/c)^2$ is negligible, because of the rapid fall of the nucleon form factors. As a matter of fact one can ignore the electric neutron form factor completely after integration.

Note that the set of data of unfolded energy-dependent charged-current quasi-elastic (CCQE) cross-section model suffer from uncertainties driven by the model dependence of the neutrino energy reconstruction. The comparison of Fig. 3 is merely indicative for illustration purposes of the kind of predictions that the present approach can provide for proper flux-averaged doubly differential cross sections. These comparison will be presented in a forthcoming presentation.

IV. CONCLUSIONS

At present there is no model able to reproduce the 2500 data points from $^{12}\mathrm{C}(e,e')$ experiments. Due to the impossibility to fit the quasi-elastic peak or other regions with the experimental accuracy, in the present approach, we have shown that instead of making an extremely detailed analysis of the particular reaction, which may be well beyond the present validation possibilities, it is possible to isolate those data contributing to the simplest possible physics we are interested in and use that information to make predictions with the maximum allowed precision, since one cannot distinguish the theoretical noise from the experimental signal.

ACKNOWLEDGMENT

This work is supported by the Spanish Dirección General de Investigación Científica y Técnica (Grant No. FIS2014-59386-P) and Agencia de Innovación y Desarrollo de Andalucía (Grant No. FQM225).

[1] V. Lyubushkin *et al.* (NOMAD Collaboration), Eur. Phys. J. C **63**, 355 (2009).
[2] A. Aguilar-Arevalo *et al.* (MiniBooNE Collaboration), Phys. Rev. D **81**, 092005 (2010).
[3] A. Aguilar-Arevalo *et al.* (MiniBooNE Collaboration), Phys. Rev. D **88**, 032001 (2013).
[4] G. A. Fiorentini *et al.* (MINERvA Collaboration), Phys. Rev. Lett. **111**, 022502 (2013).
[5] K. Abe *et al.* (T2K Collaboration), Phys. Rev. D **87**, 092003 (2013).
[6] H. Gallagher, G. Garvey, and G. P. Zeller, Annu. Rev. Nucl. Part. Sci. **61**, 355 (2011).
[7] J. A. Formaggio and G. P. Zeller, Rev. Mod. Phys. **84**, 1307 (2012).
[8] J. G. Morfin, J. Nieves, and J. T. Sobczyk, Adv. High Energy Phys. **2012**, 934597 (2012).
[9] L. Alvarez-Ruso, Y. Hayato, and J. Nieves, New J. Phys. **16**, 075015 (2014).
[10] J. E. Amaro, M. B. Barbaro, J. A. Caballero, T. W. Donnelly, A. Molinari, and I. Sick, Phys. Rev. C **71**, 015501 (2005).
[11] R. Gonzalez-Jimenez, G. D. Megias, M. B. Barbaro, J. A. Caballero, and T. W. Donnelly, Phys. Rev. C **90**, 035501 (2014).
[12] J. E. Amaro, M. B. Barbaro, J. A. Caballero, T. W. Donnelly, and C. Maieron, Phys. Rev. C **71**, 065501 (2005).
[13] J. A. Caballero, J. E. Amaro, M. B. Barbaro, T. W. Donnelly, and J. M. Udias, Phys. Lett. B **653**, 366 (2007).
[14] P. Alberto, S. S. Avancini, and M. Fiolhais, Int. J. Mod. Phys. E **14**, 1171 (2005).
[15] P. Alberto, S. S. Avancini, M. Fiolhais, and J. R. Marinelli, Phys. Rev. C **75**, 054324 (2007).
[16] R. Rosenfelder, Ann. Phys. (NY) **128**, 188 (1980).
[17] B. D. Serot and J. D. Walecka, Adv. Nucl. Phys. **16**, 1 (1986).
[18] O. Benhar, D. Day, and I. Sick, Rev. Mod. Phys. **80**, 189 (2008).
[19] A. M. Ankowski, O. Benhar, and M. Sakuda, Phys. Rev. D **91**, 033005 (2015).
[20] K. Wehrberger, Phys. Rep. **225**, 273 (1993).
[21] A. Mariano and C. Barbero, J. Phys. G **31**, 119 (2005).
[22] W. M. Alberico, A. Molinari, T. W. Donnelly, E. L. Kronenberg, and J. W. Van Orden, Phys. Rev. C **38**, 1801 (1988).
[23] K. Saito, K. Tsushima, and A. W. Thomas, Prog. Part. Nucl. Phys. **58**, 1 (2007); K. Tsushima, H. Kim, and K. Saito, Phys. Rev. C **70**, 038501 (2004).
[24] M. B. Barbaro, R. cenni, A. De Pace, T. W. Donnelly, and A. Molinari, Nucl. Phys. A **643**, 137 (1998).
[25] O. Benhar, D. Day, and I. Sick, arXiv:nucl-ex/0603032.
[26] http://faculty.virginia.edu/qes-archive/.
[27] *Lessons from the Masters: Current Concepts in Astronomical Image Processing*, edited by R. Gendler (Springer, New York, 2013).
[28] A. Bodek, S. Avvakumov, R. Bradford, and H. S. Budd, Eur. Phys. J. C **53**, 349 (2008).